Received: 10 February 2021 | Revised: 11 April 2021 | Accepted: 28 May 2021

IET Generation, Transmission & Distribution

DOI: 10.1049/gtd2.12222

The Institution of Engineering and Technology WILEY

ORIGINAL RESEARCH PAPER

Short-term reliability evaluation of integrated electricity and gas systems considering dynamics of gas flow

Sheng Wang[1] | Yi Ding[1] | Xiaoqing Han[2] | Peng Wang[3] | Lalit Goel[3] | Jien Ma[1]

[1] College of Electrical Engineering, Zhejiang University, Hangzhou, China

[2] School of Electrical and Power Engineering, Taiyuan University of Technology, Taiyuan, China

[3] Electrical and Electronic Engineering, Nanyang Technological University, Singapore, Singapore

Correspondence
Jien Ma, College of Electrical Engineering, Yuquan Campus, Zhejiang University, 38 Zheda Road, Hangzhou 310027, China.
Email: majien@zju.edu.cn

Funding information
National Key Research and Development Program of China, Grant/Award Number: 2017YFB0903400; National Natural Science Foundation China, and Joint Programming Initiative Urban Europe Call (NSFC-JPIUE), Grant/Award Number: 71961137004; National Science Foundation of China, Grant/Award Number: 71871200

Abstract

With the adoption of gas-fired units (GFU), the interaction between the electricity and gas systems has been intensified. The failure of the gas sources may lead to the insufficiency of the gas supply to the GFUs, and further result in the electricity supply shortage, threatening reliabilities of electricity and gas systems. However, compared with the electric power flow, the dynamics of the gas flow are much slower. Most of the existing studies evaluated the reliabilities of integrated electricity and gas systems (IEGS) without considering the slower dynamics of gas flow, which are not fully accurate in the short-term. This paper proposes a short-term reliability evaluation technique for IEGS considering the gas flow dynamics. Firstly, the short-term reliability models of gas sources, GFUs, and gas compressors are developed. Then, the multi-stage contingency management scheme is proposed, where gas flow dynamics are analysed for determining the time-varying load curtailments of electricity and gas. Moreover, a time-sequential Monte Carlo simulation technique is developed with the finite-difference scheme to tackle the gas flow dynamics during the short-term reliability evaluation. Finally, the proposed reliability evaluation technique is validated using an integrated IEEE reliability test system and the practical Belgium gas transmission system.

1 | INTRODUCTION

With the growing concerns towards low-carbon and sustainable development, natural gas has become a significant fossil fuel to generate electricity [1]. For example, the gas consumption from the electric power sector has increased by 22.03% in the USA in the last three years [2]. Due to this growing interdependency between electricity and gas systems, the two energy systems tend to be regarded as integrated electricity-gas systems (IEGS) for coordinated operation. This offers new possibilities to promote energy efficiency and economic production [3].

However, the interdependency also brings potential challenges to the reliable operation of IEGS. The failure triggered in the gas system may propagate to the electricity system, as the gas-fired units (GFU) rely on the timely gas supply. On 15 August, 2017 in Taiwan, China, the gas supply to the Datan power plant was interrupted, directly leading to a 4 GW electricity shortage [4]. Therefore, a comprehensive reliability evaluation is necessary for securing the reliable operation of the IEGS.

Accurately modelling the electricity and gas flows is the prerequisite for evaluating the reliability of the IEGS. The simulation of gas flow in a generalized connected gas pipeline network was introduced in [5]. The optimal power flow model in the gas system was then developed in [6], which was solved using the simplex method. The integrated electricity-gas power flow was proposed in [7], and was solved using the interior point method and heuristic algorithm in [8] and [9], respectively. Considering the multi-area characteristics and the uncertainties in the IEGS operation, the decentralized and probabilistic integrated electricity and gas power flow techniques were developed in [10] and [11], respectively.

Based on these research foundations, the reliabilities of electricity [12] and gas systems have been studied individually in the last few decades. The reliability of IEGS is to ensure that there is sufficient electricity generation, gas production, as well as transmission facilities to transport and satisfy the electricity and gas loads of consumers at various locations [13]. For the gas system, a long-term reliability evaluation method for the natural gas

pipeline networks was proposed in [14]. A simulation approach for the short-term security analysis of natural gas supply in Colombia was proposed in [15]. In recent years, these traditional reliability evaluation techniques were gradually extended and applied in the IEGS considering the interdependency between the energy systems. The impact of natural gas infrastructure on the electricity system was quantitatively studied in [16]. An analytical method for the reliability evaluation of IEGS was proposed in [17], and the influence of power-to-gas facilities was investigated. The stochastic process of IEGS components was simulated using the Monte Carlo simulation approach in [18]. A hierarchical-decoupling and impact-increment-based reliability evaluation framework for IEGS was proposed in [19]. The reliability network equivalent was used in [20] to reduce the computation burden of the reliability evaluation in IEGS.

These studies, however, focus on the long-term (time-independent) reliability evaluation techniques only. These techniques are usually applied for system planning, while not fully applicable for evaluating the short-term reliability of IEGS in the operational horizon [21]. Short-term reliability is evaluated on the operational phase under the time-varying system operating condition. The "short-term" is defined as a period ranging from several hours to one week [22]. In this timeframe, the dynamics of gas flow are significantly slower than those of electricity flow. When the gas well fails, the downstream GFUs may still be able to generate electricity for a relatively short period by utilizing the gas stored in the pipelines, which is also known as linepack [23]. It can serve as an effective buffer to mitigate the consequences of gas well failures. Consequently, using the steady-state gas flow model will lead to inaccuracies in the short-term reliability evaluation.

The dynamics of gas flow were modelled in the traditional natural gas transmission system design and simulation [24, 25]. However, it is not easy to embed it into the electricity system operation. The gas flow dynamics are governed by a set of partial derivative equations (PDE). It is difficult to obtain analytical solutions for a set of generally connected gas pipelines. Finite-difference schemes were usually adopted to discretise the PDEs into numerical equations [26]. By considering the continuity of the operating state of the gas system, [27] and [28] transferred the original time-independent integrated electricity-gas power flow optimization problem into a time-coupling optimal control problem. Furthermore, the gas flow dynamics have been considered in the unit commitment [29] and economic dispatch [30] in the IEGS under wind uncertainties. The gas flow dynamics were also used in [31] to characterize the interdependency between the electricity and gas systems.

However, these optimization models are conducted under a predefined time period. For example, the day-ahead unit commitment problem is an optimization problem over the next 24 h [32]. In the short-term reliability evaluation, however, the durations of components failures are uncertain which cannot be precisely foreseen in advance. Therefore, when the component failure occurs and transfers the IEGS into a contingency state, new techniques are required to determine the optimized operating condition of IEGS considering the gas flow dynamics, such as the time-varying power output of generators, the curtailments of electricity and gas loads etc.

Summarizing previous researches, we find that the effect of gas flow dynamics on the short-term reliability of IEGS has not been quantitatively explored. To fill the research gaps, this paper contributes in the following aspects:

1. A novel short-term reliability evaluation framework for IEGS is proposed. Compared with traditional steady-state based reliability evaluation techniques, the proposed technique is more practical in the operational phase by incorporating the gas flow dynamics.
2. Multi-state short-term reliability models for IEGS components are developed, which are capable of characterizing the time-varying state probabilities. Especially for GFUs, both the inherent failure and constraints from gas flow are considered.
3. A multi-stage contingency management scheme is proposed to determine the time-varying load curtailments, considering the interdependency between the electricity and gas systems. Both the optimal dispatch strategy and transient-state analysis (TSA) of gas flow are incorporated.
4. For evaluating the short-term reliability indices with PDEs, a time-sequential Monte Carlo simulation (TSMCS) technique is developed by embedding the finite-difference scheme into its inner loop. Several practical techniques are also developed to reduce computation time.

2 | MULTI-STATE SHORT-TERM RELIABILITY MODELS OF IEGS COMPONENTS CONSIDERING GAS FLOW DYNAMICS

As illustrated in Figure 1, in the natural gas transmission system, the gas pipelines are responsible for transporting the gas from distant gas sources, e.g. gas wells and storages, to the demands at different gas buses (GB). At the end of long gas transmission pipelines, the gas compressor might be installed to compensate for the pressure loss. The gas demand can be divided into two categories. One is the non-power gas load from residential and industrial users etc. The other is the gas consumption from GFUs, through which the electricity system is interconnected with the gas system.

The short-term reliability of gas sources, GFUs, and traditional fossil units are represented using multi-state models. The gas source at a bus usually consists of several gas wells using directional and horizontal drilling technology [33]. The GFU is also a complex system comprising many parts, and the failures of these parts may lead to a situation in which the GFU operates in a derated state [34]. Therefore, compared with the traditional binary-state model, multi-state representations are more flexible and accurate for those components in reliability evaluations [12]. The effects of gas flow dynamics on the multi-state models are presented in Figure 1. During IEGS operation, the random failures or deratings of gas sources could reduce their gas production capacities. Due to the gas flow dynamics in the transmission, such failures do not reduce the available gas injection to the downstream GFUs immediately. Incorporating the inherent failures of the GFU, it determines the dispatchable electricity

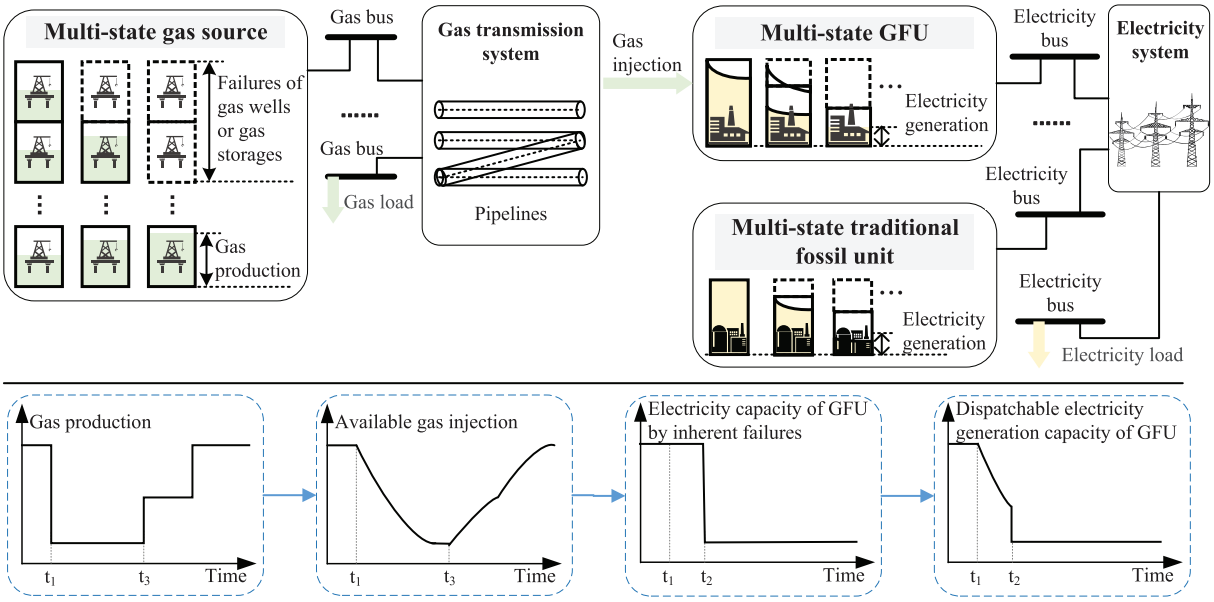

FIGURE 1 Multi-state short-term reliability model of IEGS considering the gas flow dynamics

generation capacity of the GFU in real-time. Therefore, comprehensive short-term reliability models should be developed to accurately characterize such unique and time-related behaviour of those IEGS components.

2.1 | Multi-state short-term reliability model of the gas source

Firstly, the multi-state short-term reliability model is developed to model the random failures and repairs of multiple gas wells and storages at a GB.

Generally, the reliability model of gas well or storage g at bus i uses binary-state representations $W_{i,g}^{h}$, where $h = 1$ for perfect functioning state and $h = 2$ for complete failure state, respectively [18]. During the operation, the gas well capacity$W_{i,g}(t)$ evolution in its state space produces the stochastic capacity process $W_{i,g}(t) \in \{W_{i,g}^{1}, W_{i,g}^{2}\}$ by random failures and repairs. Let $pr_{i,g}^{h}(t)$ be the probabilities of gas well g at bus i at state h:

$$pr_{i,g}^{h}(t) = \Pr\{W_{i,g}(t)=W_{i,g}^{h}\}, h = 1, 2, t \geq 0 \tag{1}$$

The state transition of the gas well is represented as a Markov process [12]. Normally all the components are assumed to be perfect functioning after commitment at the beginning of the simulation period ($W_{i,g}(t)|_{t=0} = W_{i,g}^{1}$). Then, $pr_{i,g}^{h}(t)$ can be obtained as [21]:

$$\begin{cases} pr_{i,g}^{1}(t) = \mu_{i,g}/(\lambda_{i,g} + \mu_{i,g}) + \lambda_{i,g}/(\lambda_{i,g} + \mu_{i,g})e^{-(\lambda_{i,g}+\mu_{i,g})t} \\ pr_{i,g}^{2}(t) = \lambda_{i,g}/(\lambda_{i,g} + \mu_{i,g})(1 - e^{-(\lambda_{i,g}+\mu_{i,g})t}) \end{cases} \tag{2}$$

where $\lambda_{i,g}$ and $\mu_{i,g}$ denote the failure and repair rates of gas well g at bus i, respectively. It should be noted that Equation (2) is not directly used, but implicitly contained in the TSMCS procedures in Section 4.

The state of the gas source is determined by the state combination of corresponding gas wells, and therefore its reliability can be represented using a multi-state model. The total gas production capacity takes random values from $W_i(t) \in \{W_i^{1}, \ldots, W_i^{h}, \ldots, W_i^{NH}\}$, the value of which in state h can be calculated by:

$$W_i^{h} = \sum_{g \in NG_i} W_{i,g}^{1} \tag{3}$$

where NG_i is the set of gas wells or storages in the perfect functioning state at bus i.

2.2 | Multi-state short-term reliability models of the GFU and traditional fossil unit

The dispatchable electricity generating capacities of the GFU and traditional fossil unit are both related to their inherent failures and repairs. For GFU, particularly, the capacity further relies on the gas supply from the gas transmission pipelines.

The inherent failure and repair process of GFU or traditional fossil unit is modelled as Markov process. Considering GFU l at bus i with $NH_{i,l}$ states. The electricity generating capacity for each state h ($h = 1, 2, \ldots, NH_{i,l}$) is$E_{i,l}^{h}$. The probability of the GFU being in the state h, $pr_{i,l}^{h}(t)$, can be obtained by solving the following differential equation set [21]:

$$\begin{cases} \frac{dpr_{i,l}^{h}(t)}{dt} = -pr_{i,l}^{h}(t)\sum_{h'=1}^{NH_{i,l},h' \neq h} \lambda_{h,h'} + \sum_{h'=1}^{NH_{i,l},h' \neq h} pr_{i,l}^{h'}(t)\lambda_{h',h}, \\ h = 1, 2, \ldots, NH_{i,l} \\ pr_{i,l}^{1}\Big|_{t=0} = 1, pr_{i,l}^{2}\Big|_{t=0} = \cdots = pr_{i,l}^{NH_{i,l}}\Big|_{t=0} = 0 \end{cases} \tag{4}$$

where $\lambda_{b,b'}$ is the state transition rate of the GFU from state b to b'. The state probability of traditional fossil units can also be calculated correspondingly. Similarly to Equation (2), Equation (4) is not directly solved, but its solution is implicitly contained in the TSCMS procedures in Section 4.

As mentioned, the dispatchable electricity generating capacity of GFU is further limited by the sufficiency of gas at the exact time and location. If the GFU capacity determined by the inherent failure is $E_{i,l}^{b}$, and the maximum available gas injection determined by TSA is $\overline{gi}_{i,l}(t)$, then the real-time dispatchable electricity generating capacity of GFU $E_{i,l}^{RT}(t)$ can be calculated as [8]:

$$E_{i,l}^{RT}(t) = \min\left\{\begin{array}{l} E_{i,l}^{b} \\ \left(-\beta_{i,l} + \left(\beta_{i,l}^{2} - 4\alpha_{i,l}\right.\right. \\ \left.\left.\left(\gamma_{i,l} - H_g\overline{gi}_{i,l}(t)\right)\right)^{1/2}\right)/2\alpha_{i,l} \end{array}\right\} \quad (5)$$

where $\alpha_{i,l}$, $\beta_{i,l}$, and $\gamma_{i,l}$ are the coefficients of heat rate for GFU l at bus i, respectively. H_g is the high heat value of natural gas.

2.3 | Multi-state short term reliability model of the gas compressor station

The function of the gas compressor is to uplift gas pressure to maintain the pressure level in the pipeline [23]. Different from gas sources and generating units, the performance of the gas compressor is indicated by the compression capability, which is measured by the ratio between its discharge pressure Π_j and suction pressure Π_i:

$$cr_j = \Pi_j/\Pi_i \quad (6)$$

where cr_j denotes the compression ratio of the gas compressor that is installed at bus j.

The compressors can have various failure modes, and thus affecting the maximum compression ratio CR_j. Generally, considering the gas compressor with NH_j^c states of maximum compression ratio. The state probability of the gas compressor in each state b can be calculated similar to Equation (4).

3 | MULTI-STAGE CONTINGENCY MANAGEMENT SCHEME CONSIDERING GAS FLOW DYNAMICS

During IEGS operation, failures or deratings of gas sources, GFUs, and traditional fossil units can reduce the electricity and gas capacities suddenly, and thus transfer the IEGS from the normal operating state to a contingency state. In this paper, it is assumed that the electricity and gas systems are regulated by a single system operator. In this circumstance, gas production and electricity generation should be re-dispatched coordinately. The electricity or gas loads would be curtailed, even in the worst case, to maintain a balanced operation.

Due to the slower dynamics of gas flow, the steady-state-based optimal power flow that is commonly adopted in the traditional electricity systems, is no longer suitable for evaluating the load curtailment in IEGS directly. Due to the unpredictability of components failure, it is not practical to directly embed the dynamic gas equations into the optimal power flow model and optimize over a given time period, such as in [28]. Therefore, a multi-stage contingency management scheme is proposed. Compared with traditional one-stage methods, the proposed multi-stage scheme is more flexible when duration of the contingency state is uncertain.

3.1 | Framework of the multi-stage contingency management

As outlined in Figure 2, the multi-stage contingency management scheme is developed. The IEGS initially operates in the normal state at the beginning. When failures or derations of gas sources, GFUs, or traditional fossil units occur, the IEGS may be transferred into a contingency state. The contingency management scheme begins with receiving the contingency state information, e.g., the failed generating units. The desired operating condition in the first stage is evaluated using a steady-state based integrated electricity and gas optimal power flow. Though the load curtailments are not finalized in this stage, it sets the boundary conditions for the TSA in the next stage, i.e. the nodal gas pressure or the quantity of gas supply. In the second stage, the TSA is conducted to determine the real-time operating condition of the gas system, e.g. the real-time gas load curtailment (GLC) and the available gas injection for GFUs. The latter factor is to further impose constraints on the GFU ramping, for evaluating the real-time electricity generation and electricity load curtailment (ELC) in the third stage.

3.2 | First stage: Re-dispatch in the contingency state using integrated electricity-gas optimal power flow

In the first stage, the integrated electricity-gas optimal power flow is conducted for determining the re-dispatch in the contingency state. Based on the total gas production capacities of gas sources, electricity generating capacities of GFUs and traditional fossil units, and other necessary network parameters of IEGS, the following variables in system state sequence k are calculated: (1) gas production of gas sources $w_{i,k}$; (2) active power of GFU l at bus i, $P_{i,l,k}$, and its reactive power $Q_{i,l,k}$; (3) active power of traditional fossil unit m at bus i, $P_{i,m,k}$, and its reactive power $Q_{i,m,k}$; (4) the compressor ratio of the gas compressor at bus j, cr_j; (5) ELCs at bus i, $ec_{i,k}$; (6) GLCs at bus i, $gc_{i,k}$. The objective at the first stage is to minimize the total operating cost TC_k. For the electricity and gas systems are dispatched jointly, the total operating cost includes the gas purchasing cost, the generation cost of traditional fossil units, and the interruption

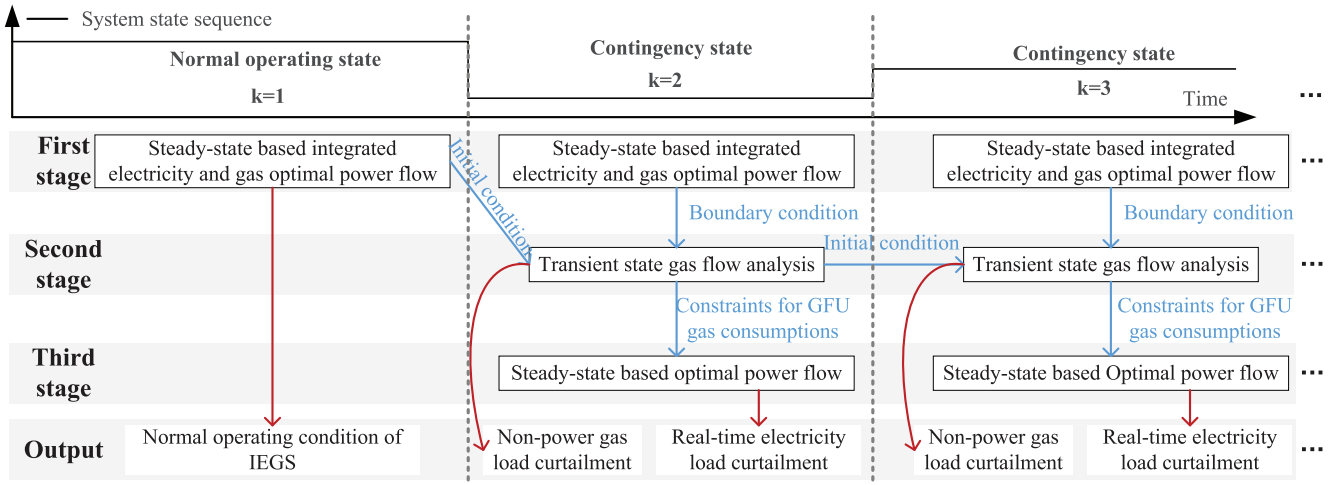

FIGURE 2 Multi-stage contingency management scheme

costs of ELCs and GLCs.

$$MinTC_k = \sum_{i\in GB}\left(\rho_i w_{i,k} + gc_{i,k}CDF_i^g(T_k)\right) + \sum_{i\in EB}\left(ec_{i,k}CDF_i^e(T_k) + \sum_{m\in NM_i} cst_{i,m}(P_{i,m,k})\right) \tag{7}$$

Subject to the following constraints:

$$\underline{W_i} \le w_{i,k} \le W_{i,k} \tag{8}$$

$$\underline{P_{i,l}} \le P_{i,l,k} \le E_{i,l,k} \tag{9}$$

$$\underline{Q_{i,l}}E_{i,l,k}/E_{i,l}^1 \le Q_{i,l,k} \le \overline{Q_{i,l}}E_{i,l,k}/E_{i,l}^1 \tag{10}$$

$$\underline{P_{i,m}} \le P_{i,m,k} \le E_{i,m,k} \tag{11}$$

$$\underline{Q_{i,m}}E_{i,m,k}/E_{i,m}^1 \le Q_{i,m,k} \le \overline{Q_{i,m}}E_{i,m,k}/E_{i,m}^1 \tag{12}$$

$$[0\ 0] \le [ec_{i,k}\ gc_{i,k}] \le [\overline{ec_i}\ \overline{gc_i}] \tag{13}$$

$$\underline{\Pi_i} \le \Pi_{i,k} \le \overline{\Pi_i} \tag{14}$$

$$\sum_{l\in NL_i}(P_{i,l,k} + jQ_{i,l,k}) + \sum_{m\in NM_i}(P_{i,m,k} + jQ_{i,m,k}) - P_i - jQ_i + ec_{i,k} - \sum_{j\in\Psi_i^e} f_{ij,k} = 0 \tag{15}$$

$$f_{ij,k} = V_{i,k}V_{j,k}((G_{ij}\cos\theta_{ij,k} + B_{ij}\sin\theta_{ij,k}) + j(G_{ij}\sin\theta_{ij,k} - B_{ij}\cos\theta_{ij,k})) \tag{16}$$

$$w_{i,k} - GL_i - \sum_{l\in NL_i} gi_{i,l,k} + gc_{i,k} - \sum_{j\in\Psi_i^g} gf_{ij,k} = 0 \tag{17}$$

$$\Pi_{j,k}^2 = \left(\Pi_{i,k}^2 - \mathrm{sgn}(\Pi_{i,k} - \Pi_{j,k})\frac{1}{C_{ij}^2}gf_{ij,k}^2\right)cr_j^2 \tag{18}$$

$$1 \le cr_j \le CR_j^b \tag{19}$$

$$[|f_{ij,k}|\ |gf_{ij,k}|] \le [\overline{f_{ij}}\ \overline{gf_{ij}}] \tag{20}$$

where Equations (8)–(12) are the electricity generation output limits on GFUs and traditional fossil units. Equation (13) is the electricity/gas load curtailment constraint. Equation (14) is the security constraints for gas pressures. Equations (15) and (16) are the AC power flow constraints. Equations (17) and (18) are the steady-state gas flow constraints, which are also known as steady-state gas Kirchhoff's current and voltage laws, respectively. Equation (19) is the boundary for gas compressors. Equation (20) is the electricity/gas power flow limit. EB, GB, NM_i, and NL_i are the sets of electricity bus (EB), GB, traditional fossil unit, and GFU at bus i, respectively. T_k is the duration of system state sequence k. ρ_i is the gas price at bus i. CDF_i^e and CDF_i^g are the electricity and gas customer damage functions (CDF). The value of electricity CDF can be found in [35]. It is associated with the customer sector, interruption duration etc. The calculation method of gas CDF can be found in [36]. Based on a survey conducted by Norway Institute for Research in Economics and Business Administration (SNF), the electricity CDF can be decoupled into each end-use of energy, and the gas CDF can be obtained by reconstructing these CDFs of end-use categories [37, 38]. $cst_{i,m}$ is the generation cost function for traditional fossil unit. $E_{i,m,k}$ is the electricity generating capacity of traditional fossil unit at system state k. $E_{i,m}^1$ is the electricity generating capacity of traditional fossil unit at perfect functioning state. CR_j^b is the maximum compression ratio at state b. $f_{ij,k}$ and $gf_{ij,k}$ are the electricity and gas flows from bus i to j. P_i and Q_i are the active and reactive power of electricity load. $gi_{i,l,k}$ is

the gas consumption of GFU. $V_{i,k}$ and $\theta_{i\,j,k}$ are the amplitude and phase angle. G_{ij} and B_{ij} are the conductivity and susceptance of the electricity branch. Ψ_i^e and Ψ_i^g are the sets of electricity branches and gas pipelines connected to bus i. $\Pi_{i,k}$ is the nodal natural gas pressure at bus i. C_{ij} is a characteristic parameter of the pipeline, depending on the length, absolute rugosity, and some other properties. sgn(x) is the signum function, where sgn(x) = 1 if $x \geq 0$, and sgn(x) = −1 if $x < 0$.

3.3 | Second stage: Operating condition of the gas system using TSA

The results from the first stage have defined the desired operating condition of IEGS, and meanwhile set the initial and boundary conditions for the second stage.

Under the assumption of isothermal gas flow and a constant compression factor in a horizontal pipeline, the following PDEs are typically used to describe the continuity and motion of the gas flow in a pipeline [39]:

$$\frac{4\omega^2}{\pi\varepsilon D^2}\frac{\partial gf}{\partial x}+\frac{\partial \Pi}{\partial t}=0 \tag{21}$$

$$\frac{\partial \Pi^2}{\partial x}+\frac{8\varepsilon\Pi}{\pi D^2}\frac{\partial gf}{\partial t}+\frac{64\varepsilon^2\omega^2 gf\,|gf|}{\pi^2F^2D^5}=0 \tag{22}$$

where Π and gf are the gas pressure and gas flow, respectively. ω is the isothermal wave speed of gas. ε is the gas density at the standard temperature and pressure, D is the diameter of the pipeline, and F is the Fanning transmission factor.

The two PDEs are formulated for each pipeline. Four values are required to characterize the state of a pipeline: the gas pressures and gas flow quantities at the beginning and end of the pipeline, respectively. Two of these four values should be specified as the boundary conditions. They can be either set as a given value, or specified implicitly in the equations associated with adjacent pipelines.

According to the types of expected boundary conditions, GBs can be divided into three categories: gas load bus, gas source bus, and other conjunction GB. For all the GBs, the gas pressures at the connecting point of pipelines are equal, as in Equation (23). For gas load buses, the gas pressures are specified as the values from the first stage, as in Equation (24). For the gas pressures obtained from the first stage are constrained within the security limits, the utilization of linepack in this stage will not violate its security constraints, either. For gas source buses and other conjunction GBs, Kirchhoff's current law holds, as in Equation (25). Noted that in the second stage, the gas Kirchhoff's laws are presented with distributed parameters. Kirchhoff's current and voltage laws are also implicitly contained in Equations (21) and (22), respectively.

$$\begin{aligned}\Pi_{ij}\Big|_{x=0}&=\Pi_{ij_1}\Big|_{x=0}\ (\forall j_1\in\Psi_i^g)\\ \Pi_{ij}\Big|_{x=0}&=cr_i^{*2}\,\Pi_{j_2i}\Big|_{x=L_{ij}}\ (\forall j_2\in\Psi_i^g)\end{aligned} \tag{23}$$

$$\Pi_{ij}\Big|_{x=0}=\Pi_{i,k}^*,\ \Pi_{ij}\Big|_{x=L_{ij}}=\Pi_{j,k}^*/cr_j^{*2} \tag{24}$$

$$w_{i,k}^*+\sum_{j\in\Psi_i^g}gf_{ji}\Big|_{x=L_{ji}}-\sum_{j\in\Psi_i^g}gf_{ij}\Big|_{x=0}=0 \tag{25}$$

where L_{ij} is the length of the pipeline from bus i to j. x^* denotes the solution of variable x obtained from the first stage.

At the beginning of the study period, the initial condition is set according to the results from the first stage when all the IEGS components are in the perfect functioning state. As the simulation proceeds, the initial condition in system state sequence k is set as the operating condition at the end of system state sequence k−1:

$$\Pi_{ij,k}(x,t)\Big|_{t=0}=\Pi_{ij,k-1}(x,t)\Big|_{t=T_{k-1}} \tag{26}$$

$$\Pi_{ij,k}(x,t)\Big|_{t=0}=\Pi_{ij,k-1}(x,t)\Big|_{t=T_{k-1}} \tag{27}$$

After solving the PDEs, the real-time pressures and quantities of gas flow can be obtained along all the pipelines. In the second stage, the gas loads are not necessarily fully satisfied, and the GFU capacities will be further constrained by the injected gas at the corresponding GB. Note that the real-time GLCs for non-power gas load $gc_i^{np}(t)$ and GFU gas requirement $gc_{i,l}^{RT}(t)$are also time-varying. The sum of them $gc_i^{RT}(t)$ can be calculated as:

$$\begin{aligned}gc_i^{RT}(t)&=gc_i^{np}(t)+\sum_{l\in NL_i}gc_{i,l}^{RT}(t)\\&=GL_i+\sum_{l\in NL_i}gl_{i,l,k}^*-w_{i,k}^*\\&\quad-\sum_{j\in\Psi_i^g}gf_{ji}\Big|_{x=L_{ji}}+\sum_{j\in\Psi_i^g}gf_{ij}\Big|_{x=0}\end{aligned} \tag{28}$$

The distribution of GLC among the non-power gas load and GFUs depends on the interruptible contracts between gas transport companies and generation utilities. In practical cases, most of the contracts entail that the GFU gas requirement is the first candidate to be curtailed, which is also the case in this paper [23, 40]:

If $gc_i^{RT}(t)\leq\sum_{l\in NL_i}gl_{i,l,k}^*$

$$gc_{i,l}^{RT}(t)=gc_i^{RT}(t)gl_{i,l,k}^*/\sum_{l\in NL_i}gl_{i,l,k}^*,gc_i^{np}(t)=0 \tag{29}$$

If $gc_i^{RT}(t)>\sum_{l\in NL_i}gl_{i,l,k}^*$

$$gc_{i,l}^{RT}(t)=gl_{i,l,k}^*,gc_i^{np}(t)=gc_i^{RT}(t)-\sum_{l\in NL_i}gl_{i,l,k}^* \tag{30}$$

3.4 | Third stage: Operating condition of the electricity system using optimal power flow

The GLC of GFU in the second stage now defines the maximum available gas injection $\overline{gi}_{i,l}$ in Equation (5):

$$\overline{gi}_{i,l}(t) = gi^{*}_{i,l,k} - gc^{RT}_{i,l}(t) \tag{31}$$

Now we can calculate the dispatchable electricity generating capacities of GFUs, $E^{RT}_{i,l}$, according to Equation (5). Based on that, the electricity system is re-dispatched to assess the actual ELC in the third stage. The objective is to minimize the electricity system operating cost EC, by controlling the GFU and traditional fossil unit generations, and the real-time ELCs ec^{RT}_{i} for each time t:

$$MinEC(t) = \sum_{i\in EB}\left(ec^{RT}_{i}(t)CDF^{e}_{i}(T_k) + \sum_{m\in NM_i} cst_{i,m}(P_{i,m}(t))\right) \tag{32}$$

Subject to Equations (9)–(13), (15), (16), and the following Equation (33):

$$[0\ -\overline{f_{ij}}] \le [ec^{RT}_{i}(t)\ f_{ij}(t)] \le [\overline{ec_i}\ \overline{f_{ij}}] \tag{33}$$

4 | SHORT-TERM RELIABILITY EVALUATION PROCEDURE

4.1 | Computation time reduction techniques in the TSMCS

The reliability evaluation of the IEGS during the operational phase is the process of predicting the reliability for the system operator and customers for a given system operating condition. TSMCS is used to sample the chronological random failures during the operation and calculate the reliability indices. In each system state simulated by the TSMCS, the optimization problem in the first stage is a non-linear programming problem, which is solved using the interior point method [41]. The continuity and motion equations in the second stage are discretised into a set of equations using a finite-difference scheme. It is implicit along the pipeline, and explicit in the time dimension [42]. The equation set is solved using the Newton–Raphson method. The gas pressure and gas flow at each time step can thus be obtained.

More specifically, the dimension of the TSA problem is analysed as follows: suppose the numbers of gas bus and gas pipeline in the gas system are NGB and NGL, respectively. Each gas pipeline is discretised into $NM-1$ pipeline sections. Thus, the total number of state variables are $2NGL\cdot NM$. The number of discretised dynamic gas flow equations is $2NGL(NM-1)$. We further assume the numbers of gas load bus, gas source bus, and gas connection bus are N_1, N_2, and N_3, respectively, $N_1+N_2+N_3=NGB$. Then, the number of equations that are formulated on the boundary conditions Equations (23) and (24) are $2NGL-NGB$and N_1, respectively. The number of equations that are formulated on the boundary conditions in Equation (25) is N_2+N_3. Thus, the number of equations equals the number of state variables, and the equation set can be solved.

Nonetheless, directly embedding the finite difference scheme into the TSMCS will introduce tremendous computational burdens. Both the convergence of TSMCS requires many simulations, and each time step entails solving a large-scale equation set. To address this issue we offer the following remarks from a practical point of view:

1. Criteria for the completion of a transient process.

With the knowledge that each transient process gradually converges to the corresponding steady-state, calculations in each system state can be avoided by setting an appropriate tolerance. Hence, a relative bound is set as the criteria for determining the completion of the transient process:

$$\left\|(\mathbf{x}(t)-\mathbf{x}(t-\Delta t))/(1+|\mathbf{x}(t-\Delta t)|)\right\|_{\infty} \le \xi_1 \tag{34}$$

where $\mathbf{x}(t)=[\Pi_{i,j,s}(t), gf_{i,j,s}(t), gc^{RT}_{i}(t)], \forall i,j,s$ is the set of IEGS state variables, and s is the index of the pipeline segment.

2. Offline contingency state database.

To avoid redundant calculation of the same system state, storing the TSA results during the first calculation is critical for reducing the computation time. Suppose the operating condition of IEGS is $\mathbf{x}_1(t)$ after the failure at t_1. When the same failure pattern occurs for the second time t_2, the operating condition $\mathbf{x}_2(t)$ can be pulled out from memories with a little modification $\mathbf{x}_2(t)=\mathbf{x}_1(t+t_1-t_2)$. However, note that the offline results should only be used when the change of system state happens after the completion of the transient process.

4.2 | Reliability evaluation procedures

The expected demand not supplied (EDNS) and loss of load probability (LOLP) are commonly adopted to characterize the reliability of the electricity system. To cope with the short-term reliability evaluation of IEGS, EDNS and LOLP are reformed as time-varying indices, and are specified for each bus, as calculated in Equations (35) and (36). Moreover, they are extended to the gas system, i.e. the expected gas demand not supplied (EGNS), and loss of gas probability (LOGP). They can be calculated using identical equations.

$$EDNS_i(t) = \left(\sum_{n=1}^{NS} ec^{RT}_{i}(t)\right)/NS \tag{35}$$

$$LOLP_i(t) = \left(\sum_{n=1}^{NS} flag(ec^{RT}_{i}(t))\right)/NS \tag{36}$$

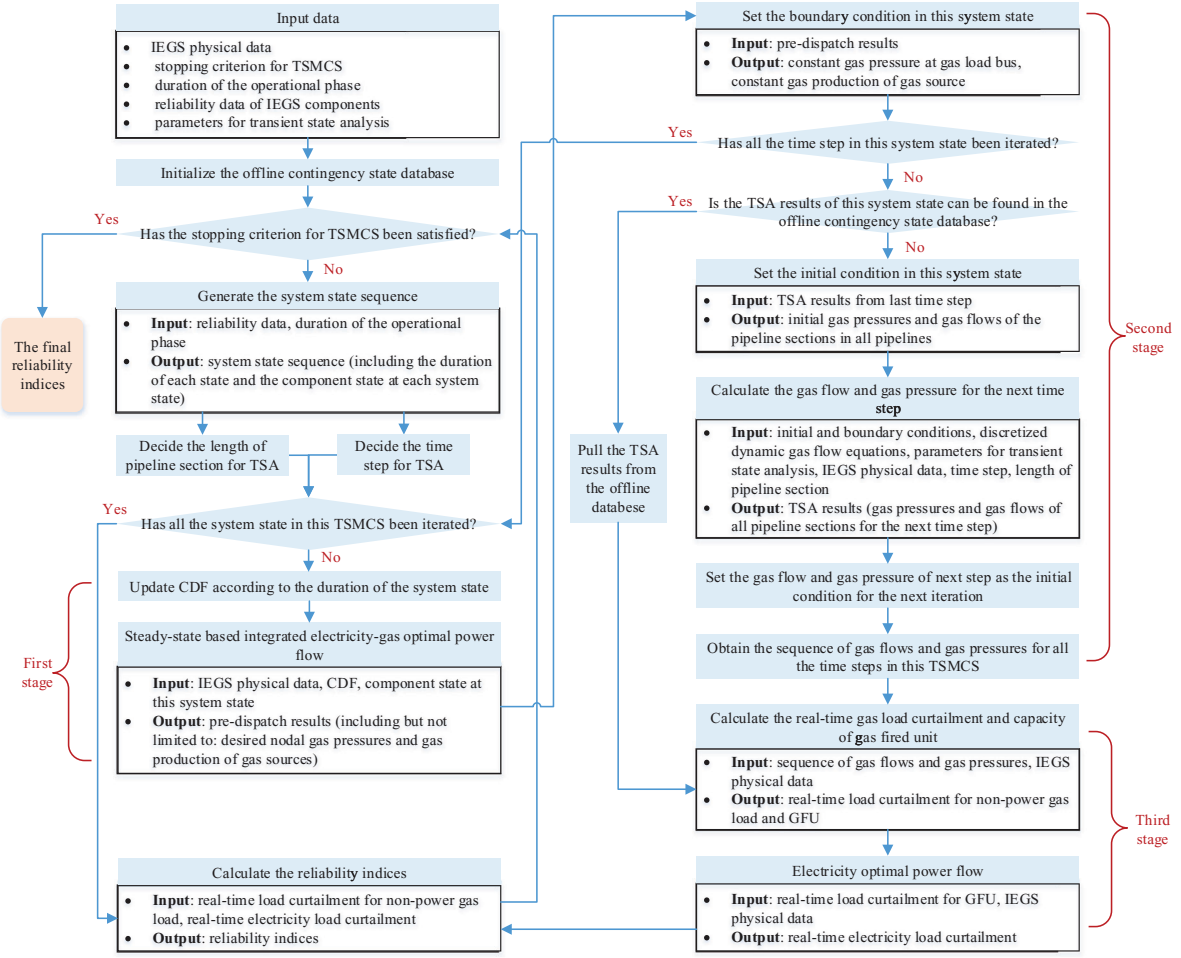

FIGURE 3 Flow chart of the short-term reliability evaluation procedures

where NS is the sampling times of the simulation. $flag(x)$ is defined as a function where $flag(x) = 1$ if $x > 0$, and $flag(x) = 0$ if $x \leq 0$. The coefficient of variation of EDNS is set as the stopping criterion for the TSMCS:

$$\sqrt{Var\left(\sum_{i\in EB} EDNS_i(t)\right)} \Big/ \sum_{i\in EB} EDNS_i(t) \leq \xi_2 \qquad (37)$$

where $Var(x)$ is the variance of x.

In summary, the short-term reliability evaluation procedure for IEGS is elaborated as follows. Moreover, the corresponding flow chart is presented in Figure 3, with input and output arguments listed in key steps.

Step 1: Calculate the operating condition of IEGS at $t = 0$ with all the IEGS components in the perfect functioning state according to Equations (7)–(20). Initialize the conditions for the transient gas flow analysis and TSMCS. Initialize the offline contingency database.

Step 2: Generate the state sequences of components and combined them into the state sequence of IEGS using the TSMCS sampling technique according to Equations (1)–(3) and (4). By this means, the electricity generating capacity, gas production capacity, and maximum compression ratio of these components in each system state can be known.

Step 3: Set the length of pipeline sections Δx_{ij} and time step Δt for the finite-difference scheme in the TSA.

Step 4: For each system state k, determine if it is in the offline contingency database. If so, use the offline data (according to Section 4.1), and go to Step 9.

Step 5: Conduct the first stage integrated optimal power flow formulated in Section 3.2. Then, the results of this pre-dispatch can be obtained, including but not limited to: the nodal gas pressures at gas load buses, p_i^* and the gas production of gas sources w_i^*.

Step 6: Set w_i^* of gas sources, p_i^* at gas load buses as the boundary conditions for TSA according to Equations (23)–(25).

Step 7: Formulate the second stage TSA for one time step Δt according to discretised Equations (21) and (22), and the pre-set initial/boundary conditions. It is essentially a set of algebraic equations. After solving the equation set, the gas flow and gas pressure in each pipeline section at the next time step can be determined. Set the solutions

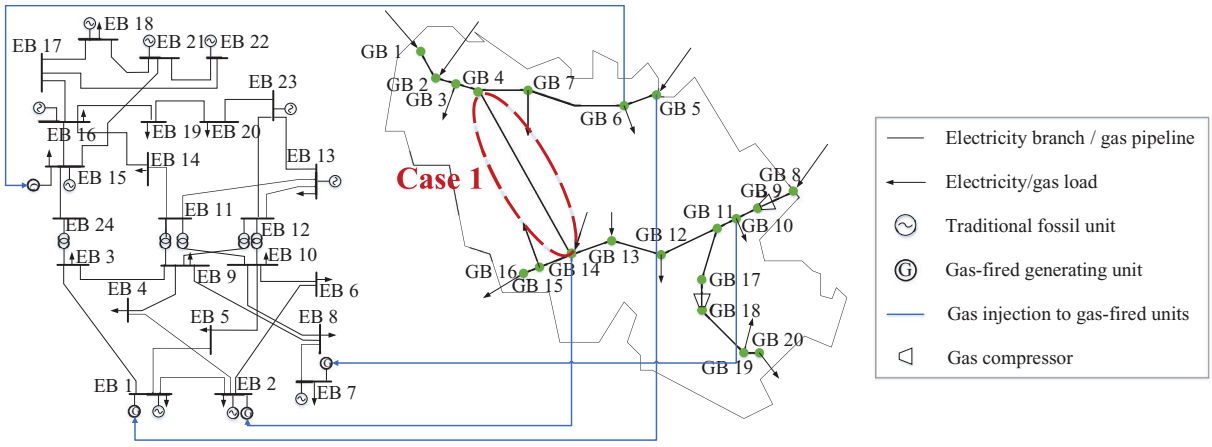

FIGURE 4 Integrated IEEE RTS and Belgium natural gas transmission system

as the initial condition for the next step according to Equations (26) and (27).

Step 8: Calculate the real-time GLCs for non-power gas load and GFU gas requirement according to Equations (28)–(30).

Step 9: Evaluate the real-time dispatchable electricity generating capacity of GFUs according to Equation (5). Conduct the optimal power flow in the electricity system according to Section 3.4.

Step 10: Repeat Steps 4–9 until it reaches the duration of system state k.

Step 11: Repeat Steps 4–10 until the whole study period ST is reached.

Step 12: Calculate the short-term reliability indices according to Equations (35) and (36). Evaluate the stopping criterion for TSMCS according to Equation (37). If it is satisfied for $t \in [0, ST]$, output the short-term reliability indices as the final results. Otherwise, begin the next simulation from Step 1.

5 | CASE STUDIES

In this section, an integrated IEEE Reliability Test System [43] and Belgium gas transmission system [6] is studied, as illustrated in Figure 4. The generating units No. 1, 2, 5, 6, 9, 10, 11, 16, 17, 18, 19, 20 in the electricity system are replaced with the GFUs of the same capacities. The coefficients of heat rate and the gas purchasing price are referred to [8]. Simulations are performed on the following three cases to validate the proposed short-term reliability evaluation technique.

5.1 | Case 1: Verification of the finite difference scheme

In this case, the finite difference scheme for solving the dynamic gas flow is verified. The pipeline from GB 4 to GB 14 is used, which is assumed to be isolated from the IEGS, as presented in Figure 4. A gas well is connected to GB 4. A gas load and a GFU are connected to GB 14, and an electricity load is further connected to the GFU. The capacities of the gas source and GFU are {6,4,2,0} Mm^3/day and 200 MW at different states. The gas pressure at GB 14 is a constant of 5.1784×10^6 Pa. The gas and electricity loads are 5 Mm^3/day and 100 MW, respectively. We assume the gas source is derated to 4 Mm^3/day at $t = 3$ h.

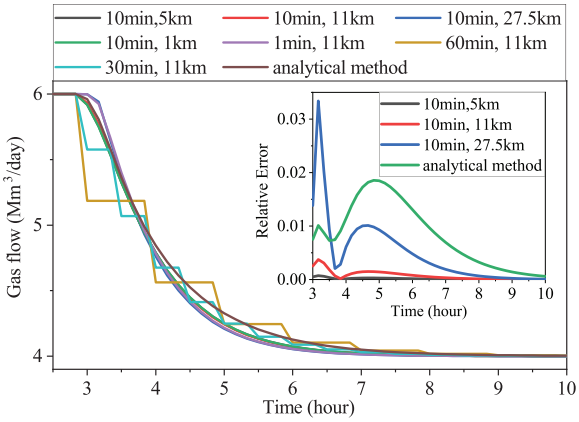

FIGURE 5 Verification of the utilized finite difference scheme

The solutions of the dynamic gas flow from $t = 3$ h to $t = 10$ h using different solvers with different settings are compared in Figure 5. Two methods, including the finite difference scheme and analytical method, as well as different time steps and pipeline section lengths for the finite difference scheme are compared. The solution procedure of the analytical method is elaborated in Appendix. Please note that since PDEs of the gas flow dynamics are non-linear, we cannot give an accurate analytical form of the solution. Instead, the Taylor expansion is used to approximate the non-linear equations [44]. Thus, the analytical solution is not fully accurate, either.

As we can see in Figure 5, the PDE solvers are all cross-checked which prove to be robust and accurate. We set the solution of finite difference scheme with 10 min time step and 1 km pipeline section as the baseline. We can find that the

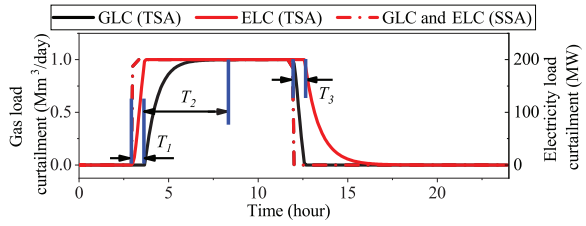

FIGURE 6 Comparison of GLCs and ELCs in TSA and SSA

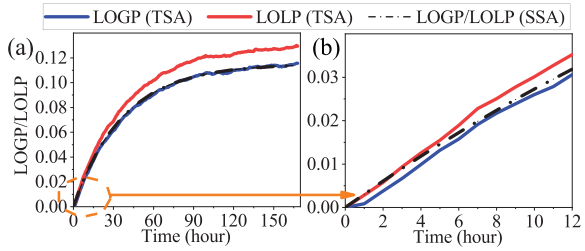

FIGURE 7 Comparison of LOGP and LOLP in TSA and SSA

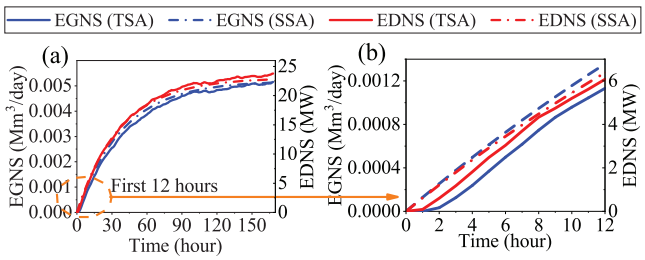

FIGURE 8 Comparison of EGNS and EDNS in TSA and SSA

analytical solver, as well as the finite difference scheme with different pipeline section lengths, can all achieve a relative error of less than 3.5%. Although we can further increase the accuracy by reducing the pipeline section length, the computation time will also increase. For example, the finite difference scheme with 10 min and 1 km takes 380 s. Therefore, we should carefully balance the length of the pipeline section and the computation time. As for the time step for the finite difference scheme, it depends on the time resolution requirement for the short-term reliability evaluation and the time constant of the gas flow dynamics. For example, we can choose a time step that less than the time constants for each pipeline, e.g. 5–30 min [29].

5.2 | Case 2: Illustration of gas flow dynamics in a single pipeline

The first illustrative case is performed on a single pipeline to demonstrate the gas flow dynamics during the contingency state, as well as the necessity to incorporate the gas flow dynamics in the short-term reliability evaluation. The study period is 168 h. The length of a pipeline section Δx= 10 km, and the time step Δt = 5 min.

As observed from the TSA results in Figure 6, the failure of the gas source is triggered at t = 3 h. Then the ELC begins to increase while the GLC remains zero within T_1. This is because the GFU's gas requirement is the first to be curtailed compared to the non-power gas load. During T_2, the insufficient quantity of gas supply exceeds the GFU gas requirement, and the gas load begins to be curtailed. Due to the slower dynamics of gas flow, part of the gas load can still be supplied by the linepack, and therefore the GLC increases gradually. The repair of the gas well completes at t = 12 h. Similarly, the gas load gradually recovers followed by the electricity load. Noted that due to the higher priority of gas load than the gas requirement of GFUs, the GLC recovers faster than it emerges. The incorporation of gas flow dynamics substantially influences the load curtailments, compared with steady-state analysis (SSA) where the state transition of IEGS can be regarded as an instant process.

Figures 7 and 8 show the influences on the short-term reliabilities by gas flow dynamics. It is worth noting in Figure 7(a) that the LOGP in TSA is almost the same as that in SSA, while LOLP in TSA is larger than that in SSA. This can be explained in Figure 6. The duration of ELC > 0 in TSA is longer than that in SSA by T_1+T_2, while the duration of GLC > 0 in TSA is the same as that in SSA. Further exploring the first 12 h in Figure 7(b), a noticeable delay for the occurrence of LOGP can be found. It can also be explained by Figure 6 that the GLC does not occur within T_1.

The EGNS and EDNS in Figure 8 present a slightly different pattern. The EGNS in TSA is smaller than that in SSA, while EDNS in TSA grows higher as time goes on. It can be explained in Figure 6. The GLC accumulated over time in TSA is smaller than that in SSA, while the ELC accumulated over time in TSA is larger than that in SSA. Similarly, as indicated by the simulations of the first 12 h in Figure 8(b), there also exists noticeable delays for EDNS and EGNS, except that the effect of gas dynamics is more obvious.

The proposed TSMCS based short-term reliability evaluation technique is compared with the analytical method, as presented in Figure 9. As we can see, the evaluation results are very close. Compared with the analytical method, the TSMCS method used in this paper is more flexible to deal with complicated compound failure modes, and does not need to pre-set the order of failure.

In summary, the following conclusions can be drawn from the above simulations: (1) the gas flow in a transmission pipeline takes from minutes to hours to stabilize. (2) With the incorporation of the gas dynamics, the LOLP increases, while the EGNS and EDNS decrease. (3) The occurrences of LOGP, EGNS, and EDNS are delayed to varying degrees, and their increasing trends are also mitigated at the beginning of the simulation.

5.3 | Case 3: Impact of gas flow dynamics on the failure propagation in a representative scenario

In this case, a representative scenario exemplifies the propagation of failures in the gas system and to the electricity system. A

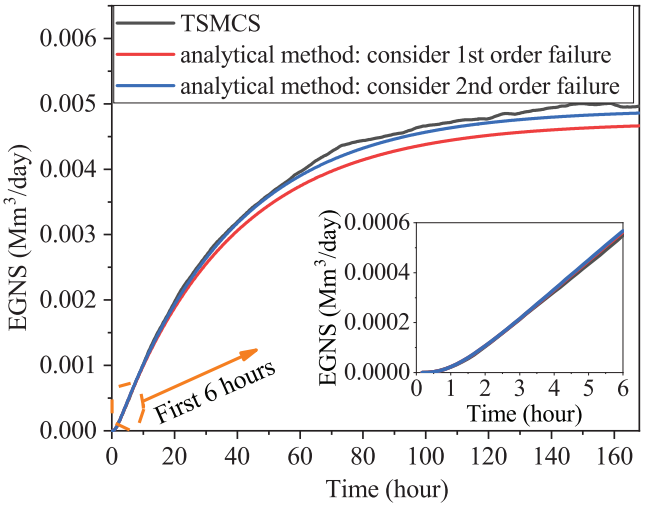

FIGURE 9 Comparison of the proposed reliability evaluation method with analytical method

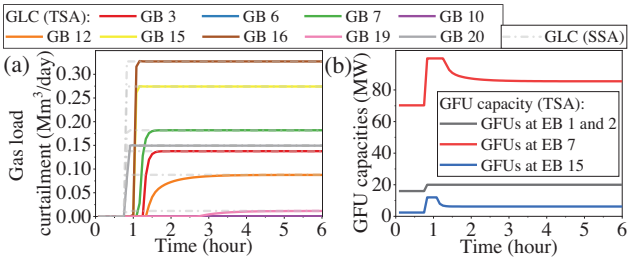

FIGURE 10 Comparison of nodal GLCs and GFU capacities in TSA and SSA

compound failure of 197 and 400 MW traditional fossil units at EB 13 and 18, and 2 Mm^3/day deration of the gas source at GB 1 is triggered at $t = 0.83$ h. The length of a pipeline section $\Delta x = 2000$ m, and the time step $\Delta t = 15$ min. The study period is 6 h. Here we define the delay time as the difference between the time of failure and time of load curtailment occurrence. Also, we define the failure distance as the minimum distance along the pipeline between the studied GB and the GB where the gas component failure has happened.

As shown in Figure 10(a), GLCs at GBs present different delay times. For example, the GLC at GB 20 increases immediately right after the failure, while GLC at GB 19 begins to increase at $t = 2.83$ h. Note that in this case, the pressures at gas load buses are controlled to be constant in the TSA. There is no monotonicity between the delay time of the GLC and the failure distance. In fact, the feature of GLC is directly determined by the inlet and outlet gas flows of the GB, which is further determined by the boundary conditions (the optimized pressures and flows at adjacent gas load buses and gas source buses, respectively). Take GB 19 and 20 for example—though they are both at the end of the same gas branch, their GLCs present entirely different temporal patterns. GB 19 and 20 are both gas load buses. Their pre- and post-fault pressures are controlled as 28.53, 26.11 bar, and 29.50, 27.53 bar, respectively. Hence, the

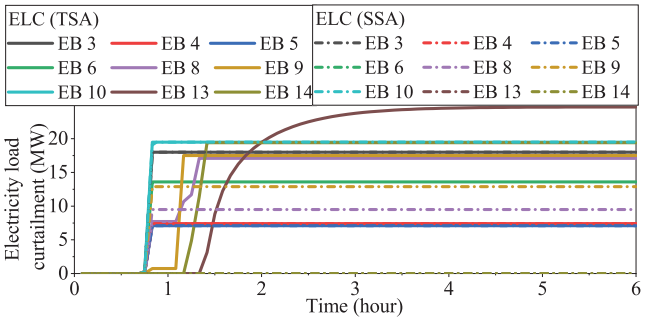

FIGURE 11 Comparison of nodal ELCs in TSA and SSA

gas flow in the pipeline between GB 19 and 20 can be soon stabilized to its steady-state value, which results in the immediate stabilization of GLC at GB 20. On the contrary, looking at the upstream GBs of GB 19, the closest gas load bus is GB 10 still a long distance away. Hence, the GLC at GB 19 takes more time to stabilize.

It is also worth mentioning that GLCs at almost all the GBs will reach their values in SSA after enough time, except GBs 6 and 10. As can be seen from Figure 4 that GBs 6 and 10 are connected with EBs 15 and 7 through GFUs. Therefore, by observing the difference between corresponding GFU capacities in TSA and the stabilized values in Figure 10(b), it can be concluded that the GLCs at GBs 6 and 10 are reduced by curtailing the gas consumption of GFUs instead.

The ELCs present a similar transient process, as shown in Figure 11. The increase in ELC is due to the time-varying GFU capacities. The ELC of EB 13 takes the longest time to stabilize, since its electricity load is mostly supplied by the GFU at EB 7. Some of the ELCs present a multi-segment feature, such as EBs 8 and 9. It is because the loads at these EBs are jointly supplied by GFUs at EB 1 or 2, and 15.

On the other hand, the stabilized value of ELCs in TSA does not necessarily equal those in SSA. For example, after considering the gas flow dynamics, the ELCs at EBs 8 and 9 have raised from 9.50 and 12.89 MW to 17.1 and 17.5 MW, respectively. This indicates that the consideration of gas dynamics and prior curtailment of GFU gas consumptions does lead to worse ELCs at some EBs eventually. Their reliabilities may also be inferior.

5.4 | Case 4: Short-term reliability indices

The short-term reliability indices for the studied IEGS are obtained in this case using TSMCS. Simulations were performed on a Lenovo laptop with an Intel Core i7-8565U 1.80 GHz and a 16GB memory. Observe from Table 1 that with the proposed technique, a computation time of 6.74 h can be achieved. It allows the system operator to evaluate the short-term reliability in the day-ahead. Moreover, TSMCS is perfect for parallel computing. The computation time can be further reduced with the implementation of production codes on a high-performance and parallel-architecture computing platform.

TABLE 1 Computation times

Proposed time reduction technique	Total (s)	For offline contingencies (s)	For TSMCS (s)
With	24,261	1747	22,514
Without	302,170	/	/

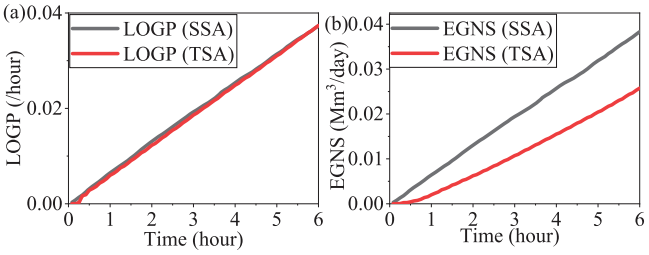

FIGURE 12 Comparison of system LOGP and EGNS in TSA and SSA

The short-term reliability of the IEGS is presented in Figures 12 and 13. On account of the same reason in Figure 6, the LOGP in TSA is almost the same as that in SSA, while the EGNS in TSA is much lower. As for the electricity system in Figure 13, the EDNS in TSA is remarkably lower than those in SSA, while the LOLP presents an opposite pattern.

Considering that load curtailments vary spatially, the reliability indices are further specified into the nodal scale. Observe from Figure 14 that the delay times of LOGP and EGNS at GBs are different. The increase in LOGP begins with GB 20, which is the same as indicated in Figure 10(a). The LOGP of GB 20 also remains the largest among all GBs during the operational phase. However, the EGNS of GB 16 begins to exceed

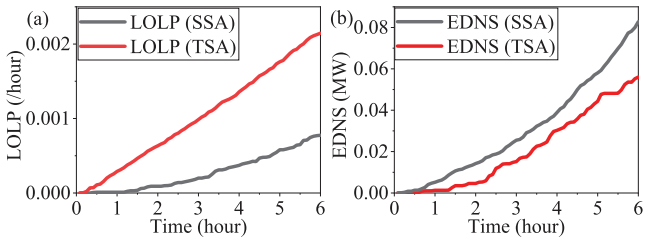

FIGURE 13 Comparison of system LOLP and EDNS in TSA and SSA

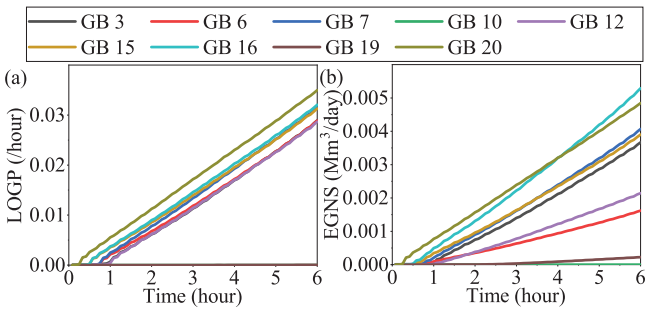

FIGURE 14 Comparison of nodal LOGP and EGNS in TSA and SSA

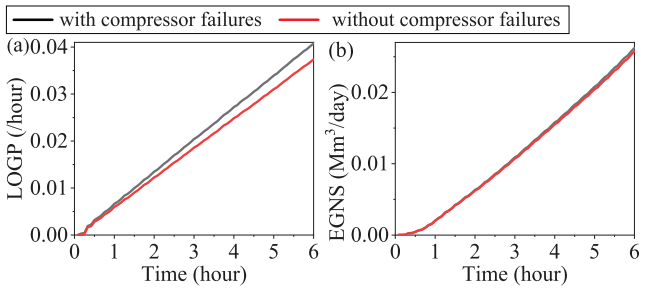

FIGURE 15 Impacts of gas compressor failures on the system LOGP and EGNS

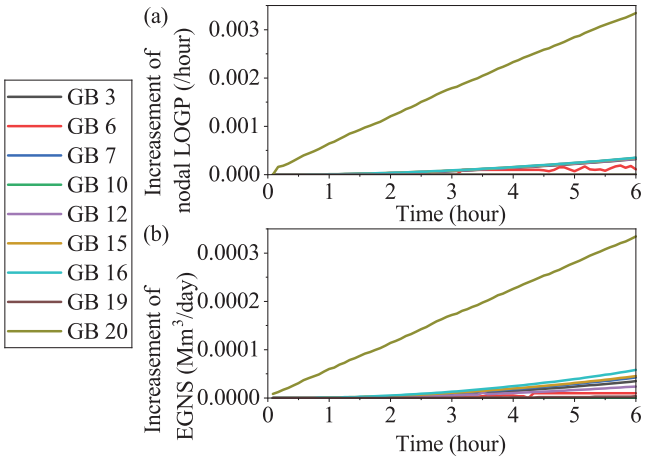

FIGURE 16 Impacts of gas compressor failures on the nodal LOGP and EGNS

GB 20 at $t = 4.25$ h. Noted that GB 16 is also at the end of another gas pipeline branch. This indicates that, although GB 20 is always most likely to be curtailed, GB 16 is also prone to suffer a more severe gas shortage after a certain time point.

5.5 | Case 5: Impacts of gas compressor failures on the short-term reliability of IEGS

In this case, the impacts of various failures of gas compressor stations on the short-term reliability of the gas system are investigated.

As presented in Figure 15, when the failures of gas compressors are considered, the LOGP and EGNS are a little higher. The differences of the reliability indices between the two scenarios also increase with time. This is because when the gas compressor fails, due to the lower gas pressures, the gas system loses part of the transmission capability, and the downstream gas loads are more likely to be curtailed. However, for there are only two compressors in the test IEGS, the influences are very limited, especially during the first several hours in the operational phase.

Compared to the scenario without compressor failure, the increment of nodal reliability indices of the gas system with gas compressor failures are further presented in Figure 16. We can

find that the LOGPs and EGNSs at almost all the GBs increases when the compressor failures are considered. Particularly, GB 20 is most vulnerable to compressor failures. Its LOGP and EGNS increase by 10.21% and 7.13% respectively, which is a very large proportion compared to the system reliability increment. It is because GB 20 is at the end of a gas pipeline branch. The gas pressure loss along this branch is quite large, so that it is highly dependent on the gas compressor at GB 18 to maintain the pressure level. Therefore, when the compressor fails, GB 18 can no longer maintain its pressure, and thus the gas load at GB 20 is curtailed. On the other hand, the failure of the gas compressor at GB 9 has limited influence on the gas supply reliabilities at GB 16, for there are alternative gas supplies from GB 13 and the pipeline from GB 4 to 14.

6 | CONCLUSION

This paper proposes a short-term reliability evaluation technique considering the gas flow dynamics. The short-term multi-state reliability models of gas sources, GFUs, traditional fossil units, and gas compressors are developed, respectively, considering the interdependency between the electricity and gas systems. A multi-stage contingency management scheme is proposed to use the gas flow dynamics to evaluate the time-varying electricity and gas load curtailments during the operation phase. TSMCS is enhanced by embedding the finite-difference scheme to solve the PDEs of gas flow, as well as to obtain the short-term reliability indices. Several practical techniques are adopted to reduce the computation time.

From the simulation results in case studies, we find that by considering the gas flow dynamics in the operational phase, the EDNS and EGNS of the IEGS can be reduced significantly. The proposed reliability evaluation technique is more accurate and practical in the operational phase compared with those that use the steady-state gas flow model. It can be further utilized to assist the system operator in short-term reliability management in practical IEGS.

ACKNOWLEDGMENTS

This work was supported in part by the National Key Research and Development Program of China under Grant 2017YFB0903400, the National Natural Science Foundation China, and Joint Programming Initiative Urban Europe Call (NSFC-JPIUE) under Grant 71961137004, and National Science Foundation of China (NSFC) under Grant 71871200.

NOMENCLATURE

Variables

$W_{i,g}^{h}$ Gas production capacity of gas well g at bus i at state h
$W_{i}^{}$ Total gas production capacity of gas wells at bus i
$E_{i,l}^{h}$ Electricity generating capacity of gas-fired unit l at but i at state h
$E_{i,l}^{RT}$ Real-time dispatchable electricity generating capacity of gas-fired unit l at bus i
$pr_{i,g}^{h}$ Probability of gas well g at bus i at state h
CR_{j}^{h} Maximum compression ratio of the gas compressor at gas bus j in state h
cr_{j} Compression ratio of the gas compressor at gas bus j
Π, gf Gas pressure and gas flow
$w_{i,k}$ Gas production of gas source at bus i at system state sequence k
$P_{i,l,k}$ Active power of gas-fired unit l at bus i at system state sequence k
$Q_{i,l,k}$ Reactive power of gas-fired unit l at bus i at system state sequence k
$ec_{i,k}$ Electricity load curtailment at bus i at system state sequence k
$gc_{i,k}$ Gas load curtailment at bus i at system state sequence k
$gi_{i,l,k}$ Gas consumption of gas-fired unit l at bus i at system state sequence k
$f_{ij,k}$ Electricity flow from bus i to j at system state sequence k
$\overline{gi}_{i,l}$ Maximum available gas injection for gas-fired unit l at bus i
gc_{i}^{np} Real-time gas load curtailment for non-power gas load at bus i
$gc_{i,l}^{RT}$ Real-time gas requirement of gas-fired unit l at bus i
gc_{i}^{RT} Real-time gas load curtailments for both non-power gas load and gas-fired units at bus i
ec_{i}^{RT} Real-time electricity load curtailment at bus i

Parameters

NH Number of state for gas well/gas-fired unit/traditional fossil unit
NG_i Set of gas wells in the perfect functioning state at bus i
EB, GB Sets of electricity/gas bus
NS Sampling times of Monte Carlo simulation
$\lambda_{h,h'}$ State transition rate from state h to h'
H_g High heat value of natural gas
ε Gas density at the standard temperature and pressure
D Diameter of the pipeline
F Fanning transmission factor
ω Isothermal wave speed of gas
TC_k Total operating cost at the first stage at system state sequence k
T_k Duration of system state sequence k
ρ_i Gas price at bus i
C_{ij} Characteristic parameter of the pipeline from bus i to j
L_{ij} Length of the pipeline from bus i to j
$V_{i,k}, \theta_{ij,k}$ Amplitude of voltage at bus i and phase angle difference between bus i and j at system state sequence k
NM_i, NL_i Sets of traditional fossil unit and gas-fired unit at bus i
Ψ_i^e, Ψ_i^g Sets of electricity branches and gas pipelines connected to bus i
$\lambda_{i,g}, \mu_{i,g}$ Failure and repair rates of gas well g at bus i

CDF_i^e,CDF_i^g	Electricity and gas customer damage functions at bus i
P_i,Q_i	Active and reactive power of electricity load at bus i
G_{ij},B_{ij}	Conductivity and susceptance of the electricity branch from bus i to j
$\alpha_{i,l}$,$\beta_{i,l}$,$\gamma_{i,l}$	Coefficients of heat rate for GFU l at bus i

Abbreviations

EB	Electricity bus
EDNS	Expected demand not supplied
EGNS	Expected gas demand not supplied
ELC	Electricity load curtailment
g, l,	Index of gas well/gas-fired unit/traditional fossil unit
GB	Gas bus
GFU	Gas-fired unit
GLC	Gas load curtailment

Indices

h, h'	Index of gas well/gas-fired unit/traditional fossil unit state
i	Index of electricity/gas bus
IEGS	Integrated electricity-gas systems
ij	Electricity branch/gas pipeline from bus i to j
k	Index of system state sequence
LOGP	Loss of gas probability
LOLP	Loss of load probability
n	Index of sampling times of Monte Carlo simulation
PDE	Partial derivative equation
s	Index of pipeline segment
SSA	Steady-state analysis
TSA	Transient-state analysis
TSMCS	Time-sequential Monte Carlo simulation

REFERENCES

1. Clegg, S., Mancarella, P.: Integrated electrical and gas network flexibility assessment in low-carbon multi-energy systems. IEEE Trans. Sustainable Energy 7(2), 718–731 (2016)
2. Monthly Energy Review. U.S. Energy Information Administration. http://www.eia.gov/totalenergy/data/monthly/#naturalgas/ (2020)
3. Hui, H., et al.: 5g network-based Internet of Things for demand response in smart grid: A survey on application potential. Appl. Energy 257, 113972 (2020)
4. Hui, H., et al.: Analysis of "8•15" blackout in Taiwan and the improvement method of contingency reserve capacity through direct load control. In: 2018 IEEE Power & Energy Society General Meeting. Portland, OR (2018)
5. Osiadacz, A.J.: Method of steady-state simulation of a gas network. Int. J. Syst. Sci. 19(11), 2395–2405 (1988)
6. De Wolf, D., Smeers, Y.: The gas transmission problem solved by an extension of the simplex algorithm. Manage. Sci. 46(11), 1454–1465 (2000)
7. Seungwon, A., Qing, L., Gedra, T.W.: Natural gas and electricity optimal power flow. In: 2003 IEEE PES Transmission and Distribution Conference and Exposition. Dallas, TX (2003)
8. Unsihuay, C., Lima, J.W.M., Souza, A.C.Z.: Modeling the integrated natural gas and electricity optimal power flow. In: *2007 IEEE Power Engineering Society General Meeting*. Tampa, FL (2007)
9. Moeini-Aghtaie, M., et al.: A decomposed solution to multiple-energy carriers optimal power flow. IEEE Trans. Power Syst. 29(2), 707–716 (2014)
10. He, Y., et al.: Decentralized optimization of multi-area electricity-natural gas flows based on cone reformulation. IEEE Trans. Power Syst. 33(4), 4531–4542 (2018)
11. Chen, S., et al.: Multi-linear probabilistic energy flow analysis of integrated electrical and natural-gas systems. IEEE Trans. Power Syst. 32(3), 1970–1979 (2017)
12. Ding, Y., et al.: Operational reliability evaluation of restructured power systems with wind power penetration utilizing reliability network equivalent and time-sequential simulation approaches. J. Mod. Power Syst. Clean Energy 2(4), 329–340 (2014)
13. AEMO, The Nem Reliability Framework. https://www.aemc.gov.au/sites/default/files/2018-11/Additional%20information%20from%20AEMO%20to%20support%20its%20Enhanced%20RERT%20rule%20change%20proposal.pdf (2018)
14. Su, H., et al.: An integrated systemic method for supply reliability assessment of natural gas pipeline networks. Appl. Energy 209, 489–501 (2018)
15. Villada, J., Olaya, Y.: A simulation approach for analysis of short-term security of natural gas supply in Colombia. Energy Policy 53, 11–26 (2013)
16. Shahidehpour, M., Yong, F., Wiedman, T.: Impact of natural gas infrastructure on electric power systems. Proc. IEEE 93(5), 1042–1056 (2005)
17. Juanwei, C., et al.: Fast analytical method for reliability evaluation of electricity-gas integrated energy system considering dispatch strategies. Appl. Energy 242, 260–272 (2019)
18. Chaudry, M., Wu, J., Jenkins, N.: A sequential Monte Carlo model of the combined gb gas and electricity network. Energy Policy 62, 473–483 (2013)
19. Lei, Y.K., et al.: A new reliability assessment approach for integrated energy systems: using hierarchical decoupling optimization framework and impact-increment based state enumeration method. Appl. Energy 210, 1237–1250 (2017)
20. Sheng, W., et al.: Reliability evaluation of integrated electricity–gas system utilizing network equivalent and integrated optimal power flow techniques. J. Mod. Power Syst. Clean Energy 7(6), 1523–1535 (2019)
21. Ding, Y., et al.: Short-term and medium-term reliability evaluation for power systems with high penetration of wind power. IEEE Trans. Sustainable Energy 5(3), 896–906 (2014)
22. Jia, H., et al.: Operating reliability evaluation of power systems considering flexible reserve provider in demand side. IEEE Trans. Smart Grid 10(3), 3452–3464 (2019)
23. Correa-Posada, C.M., Sánchez-Martín, P.: Integrated power and natural gas model for energy adequacy in short-term operation. IEEE Trans. Power Syst. 30(6), 3347–3355 (2015)
24. Shashi Menon, E.: Fluid Flow in Pipes. In: Shashi Menon, E., (ed.) Transmission Pipeline Calculations and Simulations Manual. Gulf Professional Publishing, Houston, TX (2015)
25. Yu, W., et al.: Gas supply reliability assessment of natural gas transmission pipeline systems. Energy 162, 853–870 (2018)
26. Zhou, Y., et al.: An equivalent model of gas networks for dynamic analysis of gas-electricity systems. IEEE Trans. Power Syst. 32(6), 4255–4264 (2017)
27. Zlotnik, A., et al.: Model reduction and optimization of natural gas pipeline dynamics. In: *2015 Dynamic Systems and Control Conference*. Columbus, Ohio, USA. https://asmedigitalcollection.asme.org/DSCC/proceedings-abstract/DSCC2015/57267/V003T39A002/230521 (2015)
28. Zlotnik, A., Chertkov, M., Backhaus, S.: Optimal control of transient flow in natural gas networks. In: *2015 IEEE Conference on Decision and Control*. Osaka, Japan (2015)
29. Yang, J., et al.: Effect of natural gas flow dynamics in robust generation scheduling under wind uncertainty. IEEE Trans. Power Syst. 33(2), 2087–2097 (2018)
30. Clegg, S., Mancarella, P.: Integrated modeling and assessment of the operational impact of power-to-gas (P2g) on electrical and gas transmission networks. IEEE Trans. Sustainable Energy 6(4), 1234–1244 (2015)
31. Bao, M., et al.: Nodal reliability evaluation of interdependent gas and power systems considering cascading effects. IEEE Trans. Smart Grid 11(5), 4090–4104 (2020)
32. Zhang, X., et al.: Hourly electricity demand response in the stochastic day-ahead scheduling of coordinated electricity and natural gas networks. IEEE Trans. Power Syst. 31(1), 592–601 (2016)

33. Bao, M., et al.: A multi-state model for reliability assessment of integrated gas and power systems utilizing universal generating function techniques. IEEE Trans. Smart Grid 10, 6271–6283 (2019)
34. Lisnianski, A., Frenkel, I., Ding, Y.: Multi-State System Reliability Analysis and Optimization for Engineers and Industrial Managers. Springer Science & Business Media, London (2010)
35. Wacker, G., Billinton, R.: Customer cost of electric service interruptions. Proc. IEEE 77(6), 919–930 (1989)
36. Wang, S., et al.: Operational reliability of multi-energy customers considering service-based self-scheduling. Appl. Energy 254, 113531 (2019)
37. Samdal, K., Sluttbrukeres Kostnader Forbundet Med Avbrudd Og Spenningsforstyrrelser. SINTEF energiforskning, Trondheim, Norway (2004)
38. Helseth, A., Holen, A.T.: Impact of energy end use and customer interruption cost on optimal allocation of switchgear in constrained distribution networks. IEEE Trans. Power Delivery 23(3), 1419–1425 (2008)
39. Osiadacz, A.: Simulation of transient gas flows in networks. Int. J. Numer. Methods Fluids 4(1), 13–24 (1984)
40. Alabdulwahab, A., et al.: Stochastic security-constrained scheduling of coordinated electricity and natural gas infrastructures. IEEE Syst. J. 11(3), 1674–1683 (2017)
41. Zimmerman, R.D., Murillo-Sanchez, C.E., Thomas, R.J.: Matpower's extensible optimal power flow architecture. In: *2009 IEEE Power & Energy Society General Meeting*. Calgary (2009)
42. Cameron, I.: Using an excel-based model for steady-state and transient simulation. In: *PSIG Annual Meeting*. St. Louis, MO (1999)
43. Grigg, C., et al.: The Ieee reliability test system-1996. A report prepared by the reliability test system task force of the application of probability methods subcommittee. IEEE Trans. Power Syst. 14(3), 1010–1020 (1999)
44. Yang J., Zhang N., Kang C.: Analysis theory of generalized electric circuit for multi-energy networks —Part one branch model. Autom. Electr. Power Syst. 44(9), 21–32 (2020)
45. Herrán-González, A., et al.: Modeling and simulation of a gas distribution pipeline network. Appl. Math. Modell. 33(3), 1584–1600 (2009)

How to cite this article: Wang, S., et al.: Short-term reliability evaluation of integrated electricity and gas systems considering dynamics of gas flow. IET Gener. Transm. Distrib. 15, 2857–2871 (2021). https://doi.org/10.1049/gtd2.12222

APPENDIX A: ANALYTICAL SOLUTION OF THE DYNAMIC GAS FLOW MODEL

In the motion Equation (22), the derivative term with respect to the time domain has little influence on the accuracy, especially in the long transmission pipeline with long-distance [45]. Thus, this term can be neglected. Furthermore, assume the direction of gas flow does not change during the contingency management. Consider the gas system as a dynamic system. Then, the load curtailment can be regarded as the zero-state response based on the normal operating state, under the impact of component failures. Then, we linearize the dynamic gas flow Equations (21) and (22) around the normal operating state:

$$\frac{4\omega^2}{\pi\varepsilon D^2}\frac{\partial \Delta gf}{\partial x}+\frac{\partial \Delta\Pi}{\partial t}=0 \tag{A.1}$$

$$\frac{\partial \Delta\Pi}{\partial x}+\frac{64\varepsilon^2\omega^2 gf^*}{\pi^2F^2D^5\Pi^*}\Delta gf=0 \tag{A.2}$$

where $\Delta\Pi=\Pi(x,t)-\Pi(x,0)$ and $\Delta gf=gf(x,t)-gf(x,0)$are the increments of time-varying gas pressure and gas flow with respect to their values in the normal operating state. Π^* and gf^* are the reference point of gas pressure and gas flow, respectively, which can be set as the average gas pressure and gas flow in this pipeline in the normal operating state.

Substitute Equation (A.2) into Equation (A.1), we have:

$$\frac{\partial^2\Delta\Pi}{\partial x^2}-\gamma^2\frac{\partial\Delta\Pi}{\partial t}=0 \tag{A.3}$$

where $\gamma=(\frac{16\varepsilon gf^*}{\pi F^2D^3\Pi^*})^{1/2}$.

Using Laplace transform, Equation (A.3) can be transferred into an ordinary differential equation:

$$\frac{d^2\Pi_s(x,s)}{dx^2}-\gamma^2 s\Pi_s(x,s)=0 \tag{A.4}$$

where $\Pi_s(x,s)=Laplace(\Delta\Pi(x,t))$. $Laplace(\cdot)$ is the notation of Laplace transformation.

Obtain the solution as Equation (A.5). Substitute Equation (A.5) into Equation (A.1), the general solution of gas flow can also be obtained, as in Equation (A.6).

$$\Pi_s(x,s)=\alpha e^{\gamma s^{1/2}x}+\beta e^{-\gamma s^{1/2}x} \tag{A.5}$$

$$gf_s(x,s)=s^{1/2}\gamma^{-1}(-\alpha e^{\gamma s^{1/2}x}+\beta e^{-\gamma s^{1/2}x}) \tag{A.6}$$

where α and β are the undetermined coefficients. $gf_s(x,s)$ is the Laplace transform of $gf(x,t)$. Once any two of the four boundary conditions, $\Pi_s(0,s)$,$\Pi_s(L,s)$,$gf_s(0,s)$, and $gf_s(L,s)$ are given, the coefficients can be determined.

Use Taylor expansion to approximate Equations (A.5) and (A.6). Then, the two equations can be transferred back into the time domain using inverse Laplace transform. Finally, the analytical solutions of gas pressure and gas flow can be obtained.